ACS Photonics

Article

pubs.acs.org/journal/apchd5

ITO-Free Organic Light-Emitting Transistors with Graphene Gate Electrode

Caterina Soldano,*[,†] Andrea Stefani,[†] Viviana Biondo,[†] Laura Basiricò,[‡] Guido Turatti,[†] Gianluca Generali,[†] Luca Ortolani,[§] Vittorio Morandi,[§] Giulio Paolo Veronese,[§] Rita Rizzoli,[§] Raffaella Capelli,*[,‡,⊥] and Michele Muccini[†,‡]

[†]ETC s.r.l., Via Gobetti 101, 40129 Bologna, Italy

[‡]CNR-ISMN Istituto per lo Studio di Materiali Nanostrutturati, Via Gobetti 101, 40129 Bologna, Italy

[§]CNR-IMM Istituto per la Microelettronica e i Microsistemi, Via Gobetti 101, 40129 Bologna, Italy

S *Supporting Information*

ABSTRACT: In this work, we report on the fabrication and characterization of organic light-emitting transistors (OLETs) within an indium−tin-oxide (ITO)-free platform, using graphene-based transparent conductive electrodes in place of ITO as gate electrode. A direct comparison between twin bottom-gate/top-contacts OLETs, where a standard ITO layer is replaced with a film made of a few graphene layers, shows that comparable electrical characteristics can be obtained along with a clear improvement in the electroluminescence generation characteristics. Our experimental findings pave the way to the exploitation of graphene-based transparent conductive electrodes within this class of emerging devices on flexible substrates, further promoting the novel era of flexible organic electronics.

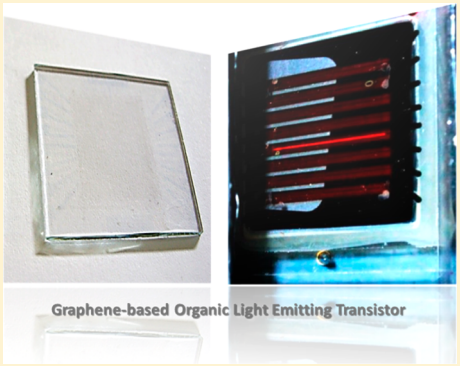

KEYWORDS: *graphene, few-layer graphene, ITO-free electronics, transparent conductive electrodes, organic electronics, organic light-emitting transistors (OLETs), flexible electronics*

Organic semiconductor-based devices such as organic light emitting diodes (OLEDs), solar cells, memories, and field-effect transistors (OFETs) are expected to reduce fabrication costs and enable novel functionalities with respect to devices and systems based on conventional materials.[1−5] In this scenario, recently developed organic light-emitting transistors (OLETs) are increasingly gaining interest within both the scientific and technological community due to their 2-fold functionality of behaving as a thin-film transistor and at the same time being capable of generating light under appropriate bias conditions.[6−10]

Nowadays, the most commonly used material as transparent conducting electrode is indium−tin-oxide (ITO). However, the exploitation of ITO is currently facing a number of challenges, mainly due to the dramatic price fluctuations as a result of the limited amount of available indium and to its intrinsic rigidity and brittleness under bending.[11] This has stimulated great efforts in the quest for alternative transparent and conductive electrode materials for various devices and the corresponding technology platforms. Several types of new transparent electrode materials may potentially replace ITO,[12] including metallic nanowires,[13] carbon nanotubes,[14−16] conductive polymers,[17,18] and graphene films.[19,20]

Graphene is a promising next-generation conducting material with the potential to replace traditional electrodes, including ITO in electrical and optical devices. A single sheet of carbon atoms, also known as graphene, is a highly transparent and conductive material. This recently discovered two-dimensional crystal[21,22] combines several key features including low sheet resistance, high optical transparency, and excellent mechanical properties,[23] offering a potentially valuable alternative to standard indium−tin-oxide. In the visible range, the transparency of graphene films decreases linearly with film thickness (and consequently number of layers). For 2 nm thick films, the transmittance is higher than 95% and remains above 70% for 10 nm films,[24,25] while for ITO a transparency in the range 60−80% is met for film thickness below 200 nm.[26] Further, the optical spectrum of graphene is quite flat between 500 and 3000 nm, with the dominant absorption below 400 nm.[27] Considering the low cost of chemically exfoliated graphene compared to ITO or carbon nanotube mats, the combination of high film conductivity, optical transparency, and mechanical stability immediately suggests employing graphene as a transparent, conductive, and flexible electrode.[24,25,28]

For example, touch screen technology (based on resistive and capacitive effects) requires a sheet resistance of 300−1500 Ω/□ at a transparency in the range 86−90%.[12] Recently, tens of centimeter long graphene films fulfilling these requirements

Received: August 11, 2014
Published: September 10, 2014

have been produced[29] and engineered into transparent electrodes for touch screen panel devices, leading to superior performances as compared to their ITO-based counterparts. In addition, ITO is a brittle material, and it has been shown that a graphene-based touch screen can withstand without breaking twice as much stress (6%, where the breaking takes place at the metal electrode and not at the graphene electrode) as ITO.

In the present work, we demonstrate the successful implementation of a graphene-based transparent conductive gate electrode in organic light-emitting transistors, along with an improvement of the overall performances compared to standard devices having an indium−tin-oxide gate electrode. Further, we show the feasibility of using graphene-based electrodes to achieve an ITO-free technology platform along with an enhancement of the performances for this particular class of emerging optoelectronic devices.

RESULTS AND DISCUSSION

Graphene and few graphene layer (FGL) with lateral dimensions of approximately 10 mm × 15 mm were grown by chemical vapor deposition (CVD) on copper substrates[30,31] (see Supporting Information for details) and then transferred onto glass substrates, where the ITO-based gate electrode has been previously removed (see Figure 1). Throughout the article, we will refer to substrates and correspondingly fabricated devices with gate electrode made of few graphene layer membranes and ITO as *G*-OLET and *I*-OLET, respectively. In our case, the indium−tin-oxide film has a thickness of 120 nm, and it has a very smooth surface (surface roughness <1−2 nm). Each substrate with FGL has been tested in order to verify the film's electrical conductivity. Electrical resistances in the range from 1 to 3 kΩ (as compared to less than 1 kΩ in the case of the corresponding ITO gate electrode) have been measured in a two-terminal electrode configuration (Figure 1c). A dielectric polymer layer (approximately 450 nm thick poly(methyl methacrylate) (PMMA)) is deposited by spin coating on both substrates (FGL and ITO), followed by a curing process under vacuum at 90 °C for 18 h. As previously demonstrated,[32] a trilayer organic stack can be exploited to generate light, which can be modulated by applying a gate voltage. In this work, a bottom-gate/top-contact (BG-TC) device configuration is used, as shown in the simplified schematics in Figure 1a. The device's active region consists of three different organic layers: the first, in direct contact with the dielectric layer, and the third layer are field-effect hole- (α,ω-disubstituted-quaterthiophene with hexyl, DH-4T, 25 nm) and electron-transporting di(perfluorohexyl-quaterthiophene, DHF-4T, 25 nm) semiconductors, respectively, whereas the intermediate layer, where the recombination and the emission processes take place, is a host−guest matrix constituted by a bis(10-hydroxybenzo[*h*]quinolinate)beryllium complex and tris(1-phenylisoquinoline)iridium [$BeBq_2$:$Ir(piq)_3$, 60 nm]. Gold drain and source electrodes (70 nm) are deposited on top of the uppermost organic layer. For the choice of n- and p-type semiconductor layers and relative considerations on the energetics of the trilayer structure, we refer the reader to ref 32 for considerations on energetics of the trilayer heterostructures (see also Figure 1b). As for the choice of the host−guest, it has been shown that the BeBq:$Ir(piq)_3$ complex is a very efficient combination with light emission in the red region of the visible spectrum.[33−35]

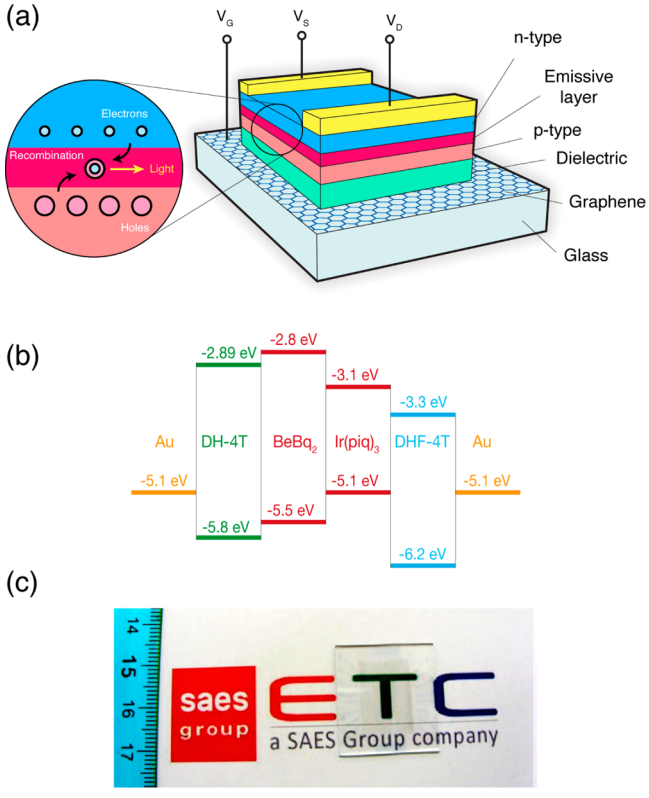

Figure 1. Organic light-emitting transistor based on a few graphene layer gate electrode. (a) Schematics of an organic light-emitting transistor, where a graphene-based electrode is used as gate and (b) relative energy diagram of the organic trilayer structure. The n- and p-type organic layers within the stack provide electrons and holes to the middle layer, where the recombination occurs, followed by light emission. (c) Optical image showing a representative substrate where the ITO gate electrode has been replaced by a graphene-based film.

Prior to fabricating organic light-emitting transistors on FGL substrates, a preliminary investigation was carried out in order to identify the concentration of $Ir(piq)_3$ within the $BeBq_2$ host matrix, leading to the maximum output signal in terms of electroluminescence signal. Trilayer structures have been fabricated on a standard glass/ITO (gate)/PMMA (450 nm) substrate by introducing in the host matrix concentrations of $Ir(piq)_3$ in the range from 2% to 16%. The experimental results indicate that a 2% $Ir(piq)_3$ concentration within the matrix leads to maximum emitted light (see Supporting Information for details).

Figure 2 shows (a, b) the typical transistor characteristics (locus and multiple output curves) with (c, d) their corresponding electroluminescence (EL) intensity (measured with a photodiode in contact with the device and with an active area larger than the device itself, a condition that ensures that all emitted photons are collected) for applied voltages up to −100 V for one of our representative devices. Solid symbols refer to *I*-OLET, while empty ones to *G*-OLET, respectively, both measured in a controlled nitrogen environment. In particular, we recall that the experimental data shown for *G*-OLET refer to a gate electrode composed of three layers of graphene, estimated based on the assumption that each graphene layer absorbs 2.3% of the impinging light at a wavelength of 550 nm[36] and determined prior to device fabrication (see Supporting Information for details). At the same reference wavelength, a thin film of ITO (120 nm) on glass has a transmittance of approximately 88%. Electrical

dx.doi.org/10.1021/ph500289s | ACS Photonics 2014, 1, 1082−1088

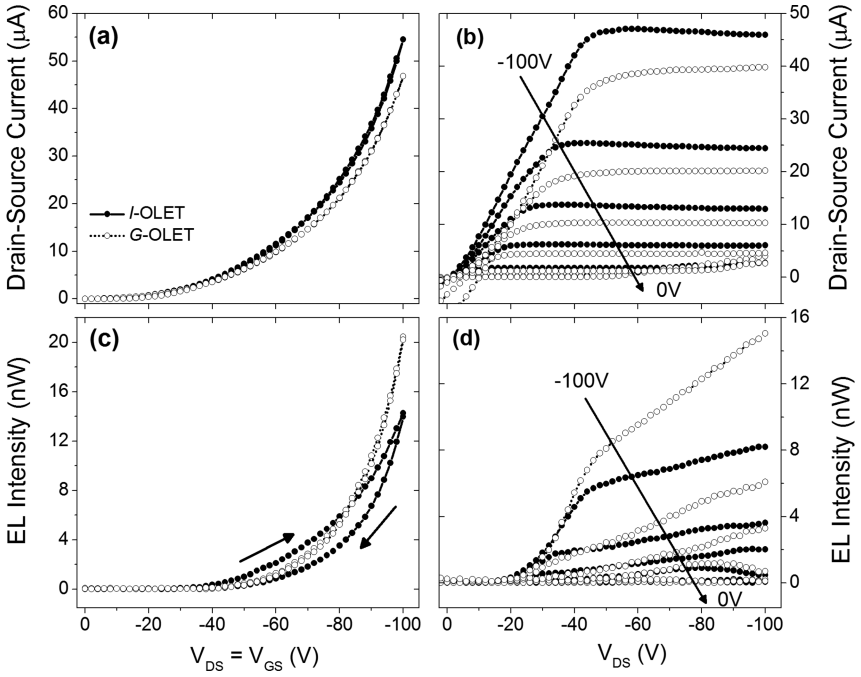

Figure 2. Electrical and optoelectronic characteristics of *I*-OLETs and *G*-OLETs. (a, b) Locus and multiple output curves of (●) *I*-OLET and (○) *G*-OLET, respectively, with (c, d) their corresponding electroluminescence curves. Arrows in (b) and (d) indicate decreasing applied constant gate bias, while arrows in (c) indicate the direction of the voltage sweeps. In terms of electrical properties, both transistors show very similar response; however in terms of emitted light we observed an increase of the optical power associated with the emitted radiation (c, d). Details about the gate leakage current contribution to the *G*-OLET drain−source current are provided in the Supporting Information.

resistance of the gate electrode has been measured in a two-terminal configuration showing values on the order of 1−3 kΩ, as compared to 0.5 kΩ for ITO in the same conditions. In terms of electrical properties, both transistors show very similar responses, with measured drain−source current of few tens of μA for applied biases V_{DS} (=V_{GS}) up to −100 V (see panel a). Threshold voltages on the order of −30 V are found for both types of devices, with estimated mobilities of 2.4×10^{-2} $cm^2/(V\ s)$ and 4.5×10^{-3} $cm^2/(V\ s)$ for hole mobility in *I*- and *G*-transistors, respectively. In both cases, multiple output curves present a typical transistor behavior characterized first by a linear region (ohmic region) up to approximately −40 V, followed by a saturation region for larger biases (and up to −100 V). We note that our *G*-device presents an unexpected and not negligible leakage current through the dielectric layer, when compared to the ITO counterpart. In this particular instance, this large (∼μA) gate current is the result of the poor quality of the FGL surface. In fact, a nonuniform flatness over the substrate is inherent to the nature of the transfer process of graphene films over large areas of a few mm^2.[37] The formation of wrinkles is often attributed to the cool-down process upon growth as a result of the difference in coefficient of thermal expansion between the graphene and the Cu substrate.[38] Inhomogeneity and kinks on the surface represent "weak spots" for the subsequent dielectric deposition, thus creating paths for the current to leak through the gate. Improvement in adhesion is under investigation. We here refer the reader to the Supporting Information (paragraph S5) for more details on surface characterization of FGL and corresponding leakage currents.

Further on, from an electrical point of view, these devices are functioning very similar to one another. On the other hand, when comparing *I*- and *G*-devices in terms of emitted light, it is necessary to distinguish between the two sets of measurements. In the case of the locus curve (Figure 2c), for the *G*-OLET we found (i) an increase of the maximum emitted power of about 50% (corresponding to the bias condition $V_{GS} = V_{DS} = -100$ V) and (ii) no hysteresis between forward and reverse sweep as compared to *I*-OLET (the direction of the sweeps is indicated). The curve shape in the case of *I*-OLET suggests that using indium−tin-oxide as a gate electrode has an overall "screening" effect on the intensity of the emitted light within the transistor structure. This is most likely the result of an induced charge polarization effect that overlaps the normal electric field operating conditions; in fact, due to the nature of the underlying ITO (*n*-type oxide), the application of a bias across the entire devices induces a polarization across each layer within the heterostructure.[39] The net consequence is to create localized charge distributions of alternatively opposite signs located at the interface between each adjacent layer and where these localized/bounded charges are not readily available for the conduction and/or the recombination process, thus limiting (in time and/or in space) the light emission. Investigation of the temperature dependence of the transport properties of these devices will surely provide some additional insight; however, at the moment, this is beyond the scope of the present work. Figure 2d shows no light emission for applied drain−source bias smaller than −20 V for both devices, while for increasing bias a rapid increase of the emitted light is detected. While in the linear region of the curves, *G*- and *I*-OLET behave similarly (same dependence and comparable values of EL), there is a dramatic difference for applied source−drain biases larger than −30/−40 V (which corresponds to the onset of the saturation region in the drain−source current modulated by the gate voltage). We experimentally observe two main features: (i) the emitted light in *G*-OLETs is systematically larger than the *I*-counterpart and (ii) it consistently rises faster than the *I*-counterpart for the same gate voltage value. In

dx.doi.org/10.1021/ph500289s | ACS Photonics 2014, 1, 1082−1088

the condition of maximum emitted light ($V_{GS} = V_{DS} = -100$ V), *G*-OLET presents almost double the power associated with the generated light as compared with the *I*-OLET. In particular, for higher source−drain voltages, a linear decrease of the emitted power is observed in Figure 2d, which corresponds to a saturation of the source−drain current in the output curves (panel Figure 2b). In this region, the curve is steeper than for the *I*-counterpart, confirming that the photon generation in *I*-OLET is at least partially limited by the polarization induced in the alternatively stacked layers upon external bias. In view of these results, we should focus our attention on the intrinsic differences between an indium−tin-oxide layer with a thickness of 120 nm and a film made of three graphene layers. The difference between *G*- and *I*-OLET devices is related to an improved extraction of the emitted light through the substrate. This is supported by the fact that very similar source−drain current values are measured in both devices, suggesting that both the gate modulation effect and the quantity of charge carriers participating in the conduction are very similar (see panel (a) in Figure 2). A change in the transmittance of the generated light through the extraction layers (ITO-PMMA vs FGL-PMMA) can be ruled out since a direct measurement of the optical transmittance of these layers shows a maximum difference of about 6% at approximately 450 nm in the visible range (see Supporting Information). This finding by itself cannot explain the difference of almost a factor of 2 in the detected light, and furthermore this difference reduces to about 2−3% if considering the spectral range of the emitted radiation (see later in the article). Thus, additional effects have to be responsible for the enhanced electroluminescence measured in *G*-OLETs, such as the following.

a. Cavity-like Effect.[40] Considering that few graphene layer behaves as a very thin and transparent metal, the entire device (FGL/dielectric/trilayer organic stacks/metal contacts) is expected to form a cavity within which the emitted radiation can propagate, possibly multiple times. Interestingly, the approximate size of the cavity (~600 nm) is close to the wavelength of the emitted light, as will be shown later. In resonant conditions, enhancement of the optical properties can take place.[41] This hypothesis is also supported by the fact that the emission takes place mostly below the (drain) electrode, as will be shown later in the article. On the other hand, this effect is not observed in *I*-OLET, because indium tin oxide is not a metal. In this case, in fact, upon electron−hole recombination and light emission in the intermediate organic layer, the radiation is reflected by the top metal electrode, then propagates through the organic layers and exits through the bottom ITO gate electrode. In this case, no enhancement of the electroluminescence is taking place.

b. Electro-optical Effects.[42] A contribution due to a variation in the electro-optical properties of FGL upon the application of an electric field cannot be *a priori* excluded, even if many of these effects are usually more dominant in the THz range, which is far from our experimental condition. In fact, upon bias optical properties of graphene have been demonstrated to be modified when surrounded by a dielectric medium. In particular, in the case of two different dielectrics (below or on top of it), variation in the optical contrast of these two media can strongly affect the propagation of radiation.

At this moment, however, it is beyond our experimental capabilities to either distinguish or quantify these two effects.

In addition, from the curves in Figure 2.a, we were able to estimate the external quantum efficiency (EQE) of our transistors, a parameter that correlates the number of available charge carriers with the number of emitted photons upon radiative recombination. Figure 3 shows the EQE for both graphene- and ITO-based transistors; corresponding drain−source current curves are also reported (right axis). We observe that (i) in the case of *G*-OLET the EQE closely follows the corresponding I_{DS} dependence and (ii) EQE value of *I*-OLET is approximately half of the corresponding G-transistor and it presents a hysteretic behavior between the forward and reverse sweep, with the latter being smaller. Both effects are directly correlated to the induced polarization in the presence of an oxide gate layer (ITO), which has the net consequence of reducing the effective electric field felt by the organic stack within the transistor. Charges are actually bounded and/or retarded at interfaces, thus being prevented from participating in the radiative recombination process, resulting in an overall reduced efficiency. These effects are absent when the gate electrode is made of few-layer graphene.

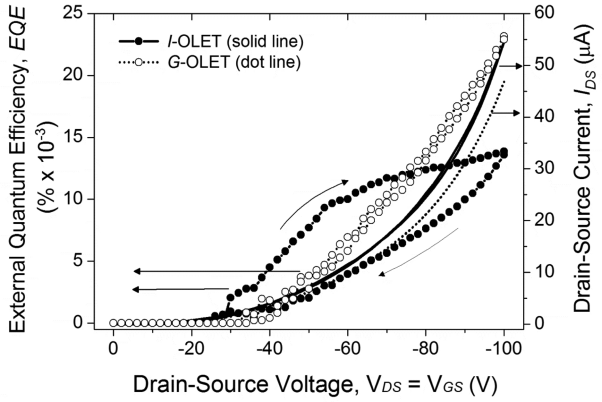

Figure 3. External quantum efficiency (EQE) for *I*-OLET and *G*-OLET (left axis) and corresponding drain−source currents (right axis) for one of our representative transistors. The net polarization effect induced in an ITO-gate device has the overall effect of preventing charges from participating in the recombination process, thus limiting the value of EQE.

Prior to proceeding to optical characterization carried out in the atmosphere, as-fabricated devices were encapsulated to prevent deterioration upon exposure to oxygen, as shown in Figure 4a (see Materials and Methods for details about the encapsulation process). Figure 4 shows the *G*-OLET in the ON-state while mounted on a sample holder along with its optical characteristics. Figure 4b is the optical image of one of our representative linear devices in the ON-state, where the transistor is biased with $V_{GS} = V_{DS} = -100$ V, a voltage condition corresponding to the maximum output emitted power. The normalized electroluminescence spectrum presents a broad peak centered at around 626 nm, which slowly decays toward the UV region of the spectrum; an additional smoothed component "centered" at around 666 nm is also present (see Figure 4c). The photoluminescence spectrum of $Ir(piq)_3$ is also reported for comparison. We were also able to determine the color coordinates associated with a graphene-based light-emitting transistor, which are $x = 0.6957$ and $y = 0.3301$, corresponding to the white circle indicated in the CIE standard color map in Figure 4d. We further studied in more detail the localization and spatial extension of the emitted light of the *G*-OLET device as a function of the applied bias. In particular, the top panel in Figure 5 shows (left) the optical image of the transistor channel (70 μm) in the *G*-OLET device, where

dx.doi.org/10.1021/ph500289s | ACS Photonics 2014, 1, 1082−1088

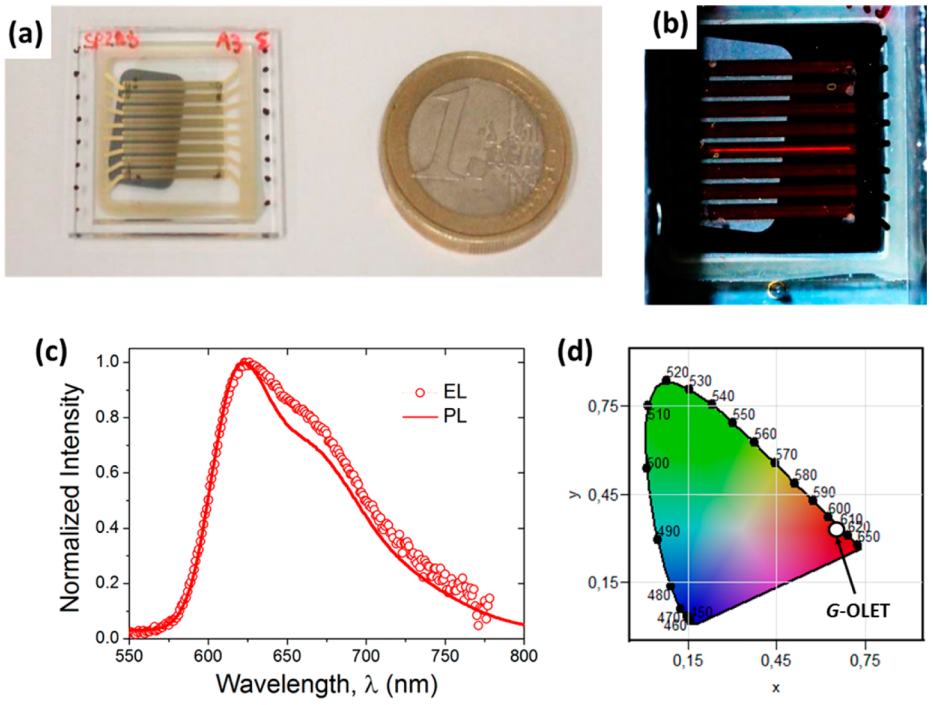

Figure 4. Optical images, emission spectrum, and color coordinates of the *G*-OLET device. Optical images of the (a) encapsulated substrate and (b) the same substrate with one G-OLET device in the ON-state. (c) Electroluminescence (EL) spectrum of one of our representative G-OLETs. The photoluminescence (PL) spectrum of $Ir(piq)_3$ is also reported. (d) XY color map plane (CIE standard) indicating the color coordinates (x = 0.6957; y = 0.3301) of our *G*-OLET (indicated by the white circle).

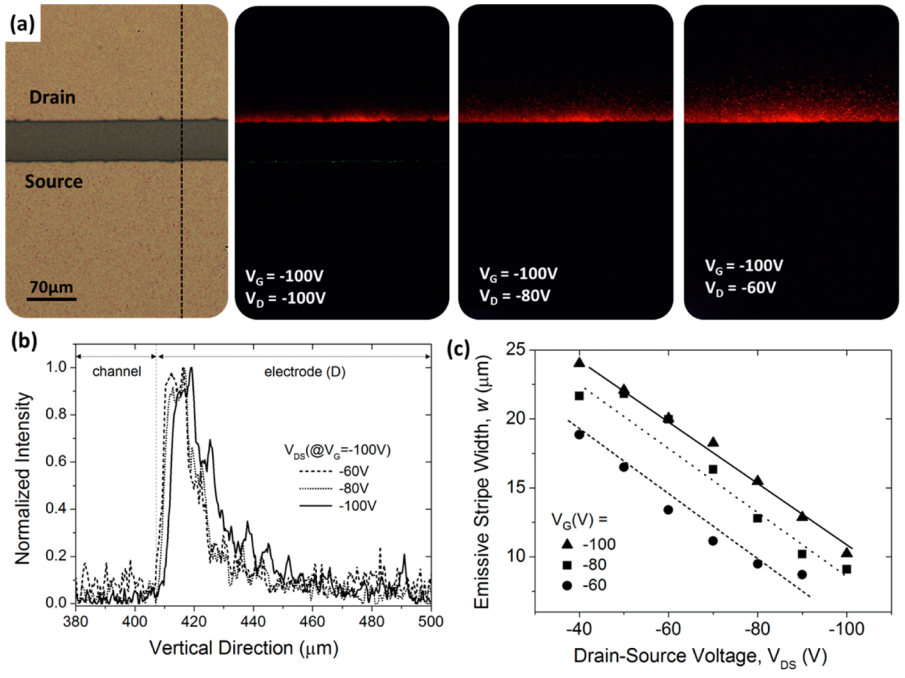

Figure 5. Optical imaging of the emitting stripe. (a) (Left to right) optical images of the device channel of one of our representative *G*-OLET devices observed from the bottom in the following conditions (left to right): no illumination, gate bias −100 V, and drain bias −100, −80, and −60 V, respectively. All images have the same scale. (b) Emitted light profile for different drain−source voltage at constant gate bias. Channel and electrode positions are also indicated. (c) Extension of the emissive stripes determined experimentally for various drain−source voltages at fixed gate biases of −100, −80, and −60 V. Dashed lines are guides to the eye.

source and drain are labeled accordingly within all panels (left to right). While keeping constant the gate voltage (−100 V), we have selected three representative drain−source voltages (−60, −80, and −100 V) for which the conditions of maximum output power are achieved. We found that for decreasing values of V_{DS} two features can be experimentally observed: (i) the extension of the emitted light (w) is localized in correspondence with the edge of the drain electrode and extends beneath

dx.doi.org/10.1021/ph500289s | *ACS Photonics* 2014, 1, 1082−1088

the electrode (without extending within the channel width) and (ii) the width of the emissive stripe becomes progressively larger. More quantitatively, we have measured for each bias condition the extension of the emissive stripe along the vertical direction (as indicated by the vertical dashed line in the left optical image in panel a) and its relative position with respect to the channel. Figure 5b and c show three representative light profiles and the width of the stripes, averaged over the entire recorded image across the channel, respectively. Thus, it is possible to controllably tune the extension of the localized emission region within the transistor beneath the drain electrode by changing the source−drain and gate biases within the transistor structure.

CONCLUSIONS

In conclusion, we have demonstrated that using graphene-based transparent electrodes is a valid and promising alternative for the fabrication of ITO-free organic light-emitting transistors. Even though the transistor behavior is very similar in both ITO- and FGL-based devices from an electrical point of view, in terms of emitted light the *G*-OLET shows a clear enhancement in terms of electroluminescence in the same operating conditions. Graphene allows for a complete replacement of current ITO transparent conductive films in multifunctional devices, overcoming the brittleness limitation inherent to ITO. Furthermore, the possibility of a large-scale CVD growth process to produce graphene allows for a practical implementation of graphene films in multiple technological platforms beyond OLETs, such as OLEDs and solar cells. This suggests the potential of implementing a large variety of electronic devices on multifunctional and flexible substrates, promoting flexible organic electronics.

MATERIALS AND METHODS

Device Fabrication. Trilayer organic heterostructure OLETs were fabricated in bottom-gate/top-contact configuration. The substrate consists of 25 mm × 25 mm square glass coated with a 120 nm thick patterned ITO serving as a gate electrode. For the fabrication of the *G*-OLET device on exactly the same glass substrates, the ITO is chemically removed in HCl solution and replaced with an FGL film. A 450 nm thick PMMA film was spin coated on the substrate and annealed in a vacuum oven at 90 °C for 18 h. The organic multilayer stack and metal electrodes were deposited by thermal evaporation by means of shadow masks in a commercial Kurt J. Lesker high-vacuum deposition chamber at room temperature at a base pressure of 10^{-6} mbar. Devices have the following characteristics: 12 mm channel width, 70 μm channel length, 0.5 mm wide source and drain electrodes. Thicknesses of dielectric, semiconducting, and metal layers were measured by means of a KLA Tencor P6 profilometer. The deposition chamber is directly connected to a glovebox to prevent sample exposure to air during the fabrication process and allow preliminary optoelectronic characterization. Devices are encapsulated inside the glovebox using a glass coverslip and an ultraviolet-cured epoxy sealant. A getter (Dryflex, provided by SAES-GETTERS) was also used to prevent any deterioration of the sample.

Electrical and Optical Characterization. Optoelectronic characterization of our devices was carried out using a SUSS probe station, coupled with a B1500A Agilent semiconductor parametric device analyzer. The measurement setup was equipped with an S1337 silicon photodiode (Hamamatsu) with a sensitivity of 0.38A W^{-1} at 600 nm, placed in contact with the devices to enable simultaneous electrical characterization and collection of all emitted photons. Electroluminescence spectra and color coordinates have been measured by a Minolta CS-2000 commercial spectro-radiometer, while optical images were taken with a Nikon Eclipse 50*i* microscope with a 10× magnification objective.

ASSOCIATED CONTENT

Supporting Information

Chemical vapor deposition growth of few-layer-graphene films, electrical characterization of single-layer OTFTs, leakage current in *G*-OLETs, substrate characterization, and optical characterization of organic light-emitting transistors. This material is available free of charge via the Internet at http://pubs.acs.org.

AUTHOR INFORMATION

Corresponding Authors

*(C. Soldano) E-mail: c.soldano@bo.ismn.cnr.it; Caterina_Soldano@saes-group.com.

*(R. Capelli) E-mail: capelli@iom.cnr.it (currently at CNR-IOM, Istituto Officina dei Materiali).

Present Address

⊥CNR - Istituto Officina dei Materiali, S.S. 14, km 163.5 in Area Science Park, I-34012, Trieste, Italy.

Notes

The authors declare no competing financial interest.

ACKNOWLEDGMENTS

C.S. would like to acknowledge financial support from FIRB project RBAP115AYN "Metal oxide nanostructures: multifunctionalities and applications". The authors acknowledge financial support from the European Marie Curie project "Training network on organic optoelectronics integrated with living systems for neuroscience investigations and applications" (OLIMPIA, FP7-PEOPLE-2012-ITN-316832).

REFERENCES

(1) Horowitz, G. Organic field effect transistors. *Adv. Mater.* **1998**, *10*, 365−377.

(2) Gomes, H. L.; Stallinga, P.; Dinelli, F.; Murgia, M.; Biscarini, F.; de Leeuw, D. M.; Muccini, M.; Müllen, K. Electrical characterization of organic based transistors: stability issues. *Polym. Adv. Technol.* **2005**, *16*, 227−231.

(3) Burroughes, J. H.; Bradley, D. D. C.; Brown, A. R.; Marks, R. N.; Mackay, K.; Friend, R. H.; Burns, P. L.; Holmes, A. B. Light-emitting diodes based on conjugated polymers. *Nat.* **1990**, *347*, 539−541.

(4) Brabec, C. J.; Sariciftci, N. S.; Hummelen, C. Plastic solar cells. *Adv. Funct. Mater.* **2001**, *11*, 15−26.

(5) Arisi, E.; Bergenti, I.; Dediu, V.; Loi, M. A.; Muccini, M.; Murgia, M.; Ruani, G.; Taliani, C.; Zamboni, R. Organic light emitting diodes with spin polarized electrodes. *J. Appl. Phys.* **2003**, *93*, 7682−7683.

(6) Muccini, M.; Koopman, W.; Toffanin, S. The photonic perspective of organic light-emitting transistors. *Laser Photonics Rev.* **2012**, *6*, 258−275.

(7) Muccini, M. A bright future for organic field-effect transistors. *Nat. Mater.* **2006**, *5*, 605−613.

(8) Rost, C.; Karg, S.; Riess, W.; Loi, M. A.; Murgia, M.; Muccini, M. Ambipolar light-emitting organic field-effect transistor. *Appl. Phys. Lett.* **2004**, *85*, 1613.

(9) Hepp, A.; Heil, H.; Weise, W.; Ahles, M.; Schmechel, R.; von Seggern, H. Light-emitting field-effect transistor based on a tetracene thin film. *Phys. Rev. Lett.* **2003**, *91*, 157406.

(10) Cicoira, F.; Santato, C. Organic light emitting field effect transistors: advances and perspectives. *Adv. Funct. Mater.* **2007**, *17*, 3421−3434.
(11) 2009 Report on "Indium Tin Oxide and Alternative Transparent Conductors Markets" by NanoMarkets: available at www.nanomarkets.net.
(12) Hecht, D. S.; Hu, L.; Irvin, G. Emerging transparent electrode based on thin films of carbon nanotubes, graphene and metallic nanostructures. *Adv. Mater.* **2011**, *23*, 1482−1513.
(13) Lee, J.-Y.; Connor, S. T.; Cui, Y.; Peumans, P. Solution-processed metal nanowires mesh transparent electrodes. *Nano Lett.* **2008**, *8*, 689−692.
(14) Wu, Z.; Chen, Z.; Du, X.; Logan, J. M.; Sippel, J.; Nikolou, M.; Kamaras, K.; Reynolds, J. R.; Tanner, D. B.; Hebard, A. F.; Rinzler, A. G. Transparent conductive carbon nanotube films. *Science* **2004**, *305*, 1273−1276.
(15) Du Pasquier, A.; Unalan, H. E.; Kanwal, A.; Miller, S.; Chhowalla, M. Conducting and transparent single-wall carbon nanotube electrodes for polymer-fullerene solar cells. *Appl. Phys. Lett.* **2005**, *87*, 203511.
(16) Ferrer-Anglada, N.; Pérez-Puigdemont, J.; Figueras, J.; Zahir Iqbal, M.; Roth, S. Flexible, transparent electrodes using carbon nanotubes. *Nanoscale Res. Lett.* **2012**, *7*, 571.
(17) Na, S.-I.; Kim, S.-S-; Jo, J.; Kim, D.-Y. Efficient and Fexible Organic Solar Cells Using Highly Conductive Polymer Anodes. *Adv. Mater.* **2008**, *20*, 4061−4067.
(18) Chang, Y.-M.; Wang, L.; Su, W.-F. Polymer solar cells with poly(3,4-ethylenedioxythiophene) as transparent electrode. *Org. Electron.* **2008**, *9*, 968−973.
(19) Pang, S.; Hernandez, Y.; Feng, X.; Müllen, K. Graphene as transparent electrode material for organic electronics. *Adv. Mater.* **2011**, *23*, 2779−2795.
(20) Zhu, Y.; Merali, S.; Cai, W.; Li, X.; Suk, W.; Potts, J. R.; Ruoff, R. S. Graphene and graphene oxide: synthesis, properties, and applications. *Adv. Mater.* **2010**, *22*, 3906−3924.
(21) Novoselov, K. S.; Geim, A. K.; Morozov, S. M.; Jiang, D.; Zhang, Y.; Dubonos, S. V.; Grigorieva, I. V.; Firsov, A. A. Electric field effect in atomically thin carbon films. *Science* **2004**, *306*, 666−669.
(22) Novoselov, K. S.; Jiang, D.; Schedin, F.; Booth, T: J.; Khotkevich, V. V.; Morozov, S. M.; Geim, A. K. Two-dimensional atomic crystals. *Proc. Natl. Acad. Sci. U.S.A.* **2005**, *102*, 10451−10453.
(23) Soldano, C.; Mahmood, A.; Dujardin, E. Production, properties and potentials of graphene. *Carbon* **2010**, *48*, 2127−2150.
(24) Blake, P.; Brimicombe, P. D.; Nair, R. R.; Booth, T. J.; Jiang, D.; Schedin, F.; Ponomarenko, L. A.; Morozov, S. V.; Gleeson, H. F.; Hill, E. W.; Geim, A. K.; Novoselov, K. S. Graphene-based liquid crystal device. *Nano Lett.* **2008**, *8*, 1704−1708.
(25) Wang, X.; Zhi, L.; Müllen, K. Transparent, conductive graphene electrodes for dye-sensitized solar cells. *Nano Lett.* **2008**, *8*, 323−327.
(26) Keum, M.-J.; Han, J.-G. Preparation of ITO thin film by using DC magnetron sputtering. *J. Kor. Phys. Soc.* **2008**, *53*, 1580−1583.
(27) Hernandez, Y.; Nicolosi, V.; Kotya, M.; Blighe, F. M.; Sun, Z.; De, S.; McGovern, I. T.; Holland, B.; Byrne, M.; Gun'ko, Y. K.; Boland, J. B.; Nirej, P.; Duesberg, G.; Krishnamuthy, S.; Goodhue, R.; Hutchison, J.; Scardaci, V.; Ferrari, A. C.; Coleman, J. N. High-yield production of graphene by liquid-phase exfoliation of graphite. *Nat. Nanotechnol.* **2008**, *3*, 563−568.
(28) Chen, J.-H.; Ishigami, M.; Jang, C.; Hines, D. R.; Fuhrer, M. S.; Williams, E. D. Printed graphene circuits. *Adv. Mater.* **2007**, *19*, 3623−3627.
(29) Bae, S.; Kim, H.; Lee, Y.; Xu, x.; Park, J.-S.; Zheng, Y.; Balakrishnan, J.; Lei, T.; Kim, H. R.; Song, Y. I.; Kim, Y.-J.; Kim, K. S.; Ozyilmaz, B.; Ahn, J.-H.; Hee, B.; Iiijima, S. Roll-to-roll production of 30-in. graphene films for transparent electrodes. *Nat. Nanotechnol.* **2010**, *5*, 574−578.
(30) Tao, L.; Lee, J.; Chou, H.; Holt, M.; Ruoff, R. S.; Akinwande, D. Synthesis of high quality monolayer graphene at reduced temperature on hydrogen-enriched evaporated copper (111) films. *ACS Nano* **2012**, *6*, 2319−2325.
(31) Ortolani, L.; Cadelano, E.; Veronese, G. P.; Degli Esposti Boschi, C.; Snoeck, E.; Colombo, L.; Morandi, V. Folded graphene membranes: mapping curvature at the nanoscale. *Nano Lett.* **2012**, *12*, 5207−5212.
(32) Capelli, R.; Toffanin, S.; Generali, G.; Usta, H.; Facchetti, A.; Muccini, M. Organic light-emitting transistors with an efficiency that outperforms the equivalent light-emitting diodes. *Nat. Mater.* **2010**, *9*, 496−503.
(33) Park, T. J.; Jeon, W. S.; Choi, J. W.; Pode, R.; Jang, J.; Kwon, J. H. Efficient multiple triplet quantum well structures I organic light emitting devices. *Appl. Phys. Lett.* **2009**, *95*, 103303.
(34) Huang, J.; Watanabe, T.; Ueno, K.; Yang, Y. Highly efficient red-emission polymer phosphorescent light-emitting diodes based on two novel tris(1-phenylisoquinolinato-C2,*N*)iridium(III) derivatives. *Adv. Mater.* **2007**, *19* (6), 739−743.
(35) Jeon, W. S.; Park, T. J.; Kwon, J. H. Highly efficient simple-structure red phosphorescent OLEDs with an extremely low doping technology. *J. Inf. Disp.* **2009**, *10*, 87−91.
(36) Nair, R.; Blake, P.; Grigorenko, A. N.; Novoselov, K. S.; Booth, T. J.; Stauber, T.; Peres, N. M. R.; Geim, A. K. Fine structure constant defines visual transparency of graphene. *Science* **2008**, *320*, 1308.
(37) Li, X.; Zhu, Y.; Cai, W.; Borysiak, M.; Han, B.; Chen, D.; Piner, R. D.; Colombo, L.; Ruoff, R. S. Transfer of large-area graphene films for high-performance transparent conductive electrodes. *Nano Lett.* **2008**, *9*, 4359−4363.
(38) Obraztsova, A. N.; Obraztsova, E. A.; Tyurnina, A. V.; Zolotukhin, A. A. Chemical vapor deposition of thin graphite films of nanometer thickness. *Carbon* **2007**, *45*, 2017−2021.
(39) Hwang, D. K.; Oh, M. S.; Hwang, J. M.; Kim, J. H.; Im, S. Hysteresis mechanisms of pentacene thin-film transistors with polymer/oxide bilayer gate dielectrics. *Appl. Phys. Lett.* **2008**, *92*, 013304.
(40) Engel, M.; Steiner, M.; Lombardo, A.; Ferrari, A. C.; Löhneysen, H. V.; Avouris, Ph.; Krupke, R. Light-matter interaction in a microcavity-controlled graphene transistor. *Nat. Commun.* **2012**, *3*, 906.
(41) Kleppner, D. Inhibited spontaneous emission. *Phys. Rev. Lett.* **1981**, *47*, 233−236.
(42) Zhu, B.; Ren, G.; Zheng; Lin, Z.; Jian, S. Tunable absorption in a dielectric-graphene-metal groove-grating absorber. *Opt. Commun.* **2013**, *308*, 204−210.